GSI Annual Report 2006 (extracts)

Doubly magic ^{270}Hs

J. Dvorak[1], R. Krücken[1], F. Nebel[1], Z. Novackova[1] , A. Semchenkov[1, 2], A. Türler[1], B. Wierczinski[1], A. Yakushev[1], W. Brüchle[2], E. Jäger[2], M. Schädel[2], B. Schausten[2], E. Schimpf[2], M. Chelnokov[3], V. Gorshkov[3], A. Kuznetsov[3], A. Yeremin[3], R. Dressler[4], Ch. E. Düllmann[5, 6], K. Eberhardt[7], P. Thörle[7], Y. Nagame[8], Z. Qin[2, 9], M. Wegrzecki[10]

[1]TU Munich, Garching, Germany; [2]GSI, Darmstadt, Germany; [3]JINR, Dubna, Russia; [4]PSI, Villigen, Switzerland; [5]LBNL, Berkeley, CA, USA; [6]UC Berkeley, CA, USA; [7]U Mainz, Germany; [8]JAEA, Tokai-mura, Japan; [9]IMP, Lanzhou, P. R. China; [10]ITE, Warsaw, Poland

Superheavy elements owe their existence exclusively to nuclear shell effects which stabilize them against spontaneous fission (SF). Theoretical predictions locate the center of stability at the hypothetical doubly-magic spherical nucleus with Z=114 and N=184 [1]. Calculations with the inclusion of higher orders of deformation [2] suggest the ground state shell correction energy of deformed nuclei around Z=108 and N=162 to reach values as large as for ^{298}114. The increased stability leads to local minima at the N=162 neutron shell and a large difference in Q_α values between Ds and Hs isotones. This is clearly visible in Figure 1, but so far no experimental α–decay energies are available for N=162 nuclei.

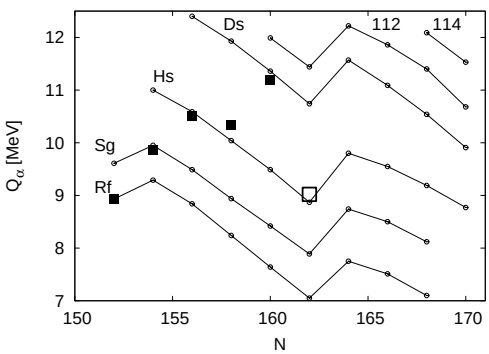

Figure 1: Q_α values from theoretical calculations and experimental data; the value for ^{270}Hs (open square) is from this work.

In [3, 4], two decay chains were tentatively assigned to ^{270}Hs based on the previously reported decay properties. However, this tentative assignment was not conclusive as the reported ^{270}Hs decay chains, consisting of α–α–SF decay sequences, were very similar to the ones assigned to ^{269}Hs. In this work we report the first synthesis and identification of the even-even nucleus ^{270}Hs and the observation of its α–decay to ^{266}Sg [5]. Contrary to earlier reports [6,7] ^{266}Sg is not decaying by α–particle emission but by SF with a relatively short half-life.

A rotating ^{248}Cm target was bombarded with a $^{26}Mg^{5+}$ ion beam at the UNILAC, GSI Darmstadt. Beam energies of 145 MeV and 136 MeV (center of target) were used to produce Hs isotopes in the 5n and 4n evaporation channels, respectively. Typical beam intensities on target were 0.8 particle-μA. Integrals of 1.46×10^{18} and 2.02×10^{18} $^{26}Mg^{5+}$ ions were accumulated at 145 and 136 MeV, respectively. An efficient rapid chemical separation method [3] together with the on-line detection system COMPACT [8] was used for the isolation and detection of Hs.

Seven decay chains attributed the decay of ^{269}Hs are described in [9]. Four α–SF chains exhibit a narrow distribution of α–particle energies with E_α=8.89±0.03 MeV. They were terminated by SF with an average lifetime of ~0.5 s. Three out of four chains were detected at the lower beam energy at the expected maximum of the 4n evaporation channel. This sequence is different from all known decay patterns. As the detection efficiency for an α-particle is 80%, there is a less than 0.1% probability that these observed α–SF chains are incomplete α–α–SF ones, where always the same α–particle was missed. We assign these four chains to the decay of the new isotope ^{270}Hs and its daughter ^{266}Sg. From the measured data Q_α=9.02±0.03 MeV and a half-life of 22 s for ^{270}Hs were derived. Measured decay properties of the observed isotopes are summarized in Tab 1.

Tab.1. Decay properties of Hs and Sg nuclei.

Z	*A*	Decay mode	Half-life	E_α
108	269	α	–	9.07±0.03 8.92±0.03
108	270	α	–	8.89±0.03
106	265	α	$14.9^{+9.1}_{-4.1}$ s	8.68±0.04
106	266	SF	444^{+444}_{-148} ms	

The α–decay energy of doubly-magic ^{270}Hs is in good agreement with theoretical calculations, which take into account shell stabilization of deformed nuclei. ^{270}Hs is the first experimentally observed even-even nucleus on the predicted N=162 neutron shell.

References

[1] A. Sobiczewski, Acta Phys. Pol. B 29, 2191 (1998).
[2] Z. Patyk *et al*., Nucl. Phys. A 533, 132 (1991).
[3] Ch.E. Düllmann *et al*., Nature 418, 859 (2002).
[4] A. Türler *et al*., Eur. Phys. J. A 17, 505 (2003).
[5] J. Dvorak *et al*., Phys. Rev. Lett. 97, (2006) 242501.
[6] Yu.A. Lazarev *et al*., Phys. Rev. Lett. 73, 624 (1994).
[7] A. Türler *et al*., Phys. Rev. C 57, 1648 (1998).
[8] J. Dvorak *et al*., GSI Report 2004, p. 183.
[9] J. Dvorak *et al*., GSI Report 2004, p. 71.

Radiochemical search for ^{268}Hs with COMPACT

J. Dvorak[1], R. Krücken[1], Z. Novackova[1], R. Schuber[1], A. Semchenkov[1,2], A. Türler[1], A. Yakushev[1], W. Brüchle[2], Ch.E. Düllmann[2], E. Jäger[2], M. Schädel[2], B. Schausten[2], E. Schimf[2], Z. Qin[2,3], R. Dressler[4], A. Kuznetsov[5], M. Chelnokov[5], K. Eberhardt[6], P. Thörle[6], and Y. Nagame[7]

[1]TU München, Germany; [2]GSI, Darmstadt, Germany; [3]IMP, Lanzhou, P. R. China; [4]PSI, Villigen, Switzerland; [5]JINR, Dubna, Russian Federation; [6]U Mainz, Germany; [7]JAEA, Tokai-mura, Japan

A rapid radiochemical technique has successfully been used to discover doubly-magic ^{270}Hs [1]. The experimental setup, based on the detection system COMPACT is described in [2]. Several successful experiments were done in the last three years [1, 3] at GSI. Here we present our recent experiment aimed at the chemical separation of ^{268}Hs, produced in the nuclear reaction ^{248}Cm(^{25}Mg, xn)$^{273-xn}$Hs. The nuclide ^{268}Hs is unknown. It is expected to decay by α-particle emission with a half-life of less than one second to 37-ms spontaneously fissioning ^{264}Sg. To be sensitive to such short-lived isotopes, the overall transport time of produced Hs nuclides from the target to our detection system was minimized and a value of less than 1 s was reached.

There are two main contributions to the overall transport time. These are the time necessary for (i) completion of the chemical reaction and (ii) transport of the nuclides. Chemical reactions can be accelerated by increasing the temperature. In our experiment, the recoil chamber and quartz filter, where oxidization occurs, were heated to 400 °C and 650 °C, respectively. To minimize the transport time, the distance between the recoil chamber and the detector setup has to be minimized. Because of the high radiation close to the target during irradiation, the chemical detection system is usually placed in separate room behind a thick concrete wall. This, however, increases the length of the transport line up to tens of meters, preventing the investigation of short-lived nuclei. Placing the COMPACT, surrounded by shielding, directly in the irradiation cave has allowed reduction of the transport line length to 4 m. This corresponds to a transport time of less than one second. The shielding of the COMPACT consisted of a 40-cm thick concrete wall, a 15-cm thick boron-paraffin layer, and a 7-cm thick Pb layer. This shielding proved to be satisfactory, as no electronic noise was observed and the background of events detected in the detector did not increase significantly compared with previous studies, when COMPACT was located outside of the irradiation cave. The experiment was operated remotely from the experiment control room.

With beam intensities of 1.5 particle-μA, an integral of 3.61×10^{18} particles was accumulated during nine days of irradiation. The lab-frame beam energy in the center of the target was 140 MeV, where HIVAP predicts the maximum cross section of $\sim$1 pb for ^{268}Hs. No events that could be attributed to the decay of ^{268}Hs or ^{269}Hs were detected.

For cross section calculations of the short-lived ^{268}Hs, knowledge of the mean transport time is necessary. This was estimated from measurements with short-lived Os isotopes. In bombardments of an enriched ^{152}Gd target with a chopped (1 s on/59 s off) ^{25}Mg beam, the isotopes ^{171}Os and ^{172}Os with half-lives of 8.3 and 19.2 seconds, respectively, were produced. The time dependence of the counting rate of the ^{171}Os and ^{172}Os decays was examined and is presented in Figure 1.

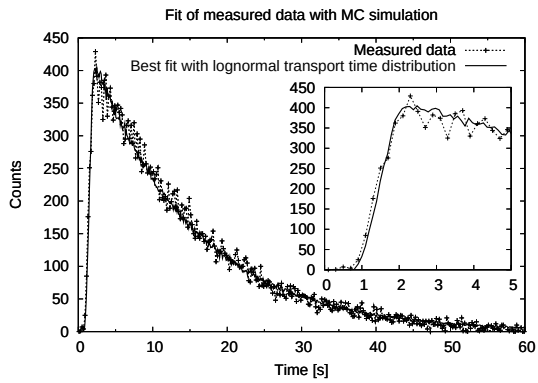

Figure 1: Time dependence of detected $\alpha-$decays of ^{171,172}Os in the detector and fit from a Monte Carlo simulation. Zero corresponds to the start of the irradiation.

A Monte Carlo simulation was performed, modelling the transport of the activity in the transport line. A lognormal shape of the transport time distribution was deduced from this model. We determined the parameters from a best fit procedure of the observed time dependence of detected $\alpha-$decays. A mean transport time of $\sim$ 1 second was calculated, in agreement with expectations.

Because the transport time is of the same order as the expected half-live, the overall detection efficiency depends on the half-life of the nuclide. A one event cross section limit of 0.8 picobarn (63.2% c.l.) has been reached for Hs isotopes with an assumed half-life of one second in this experiment. We conclude that the chemical approach allows the investigation of Hs isotopes with a half-life of one second below the one picobarn level.

References

[1] J. Dvorak *et al.*, Phys. Rev. Lett. 97 (24) (2006) 242501.

[2] J. Dvorak *et al.*, GSI Sci. Rep. 2004, p. 183

[3] J. Dvorak *et al.*, GSI Sci. Rep. 2004, p. 71

Fast electrochemical deposition of Bismuth

H. Hummrich, J.V. Kratz
Institut für Kernchemie, Johannes Gutenberg-Universität Mainz, Germany

Fast electrochemical deposition is a promising method for the aqueous chemistry of the superheavy elements [1]. To perform electrodeposition experiments, the knowledge of basic electrochemical parameters like deposition potentials and the deposition velocity is necessary. To prepare experiments with element 115, its homolog Bi was investigated.

Experiments were performed with carrier free ^{212}Bi ($t_{1/2}$ = 60 min, E_γ = 727 keV). 1 ml of a solution of ^{212}Pb in 0.5 M HCl was obtained via the emanation method [2]. The solution was passed through a column (d = 8 mm, l = 15 mm) filled with the cation exchanger Dowex 50x8 (100 - 200 mesh). Under the given conditions ^{212}Pb is retained, whereas ^{212}Bi forms an anionic chloro complex and passes the column. A total elution volume of 2 ml was sufficient to elute 90 % of the activity. The eluate was evaporated to dryness and dissolved in 1 ml 0.1 M HCl.

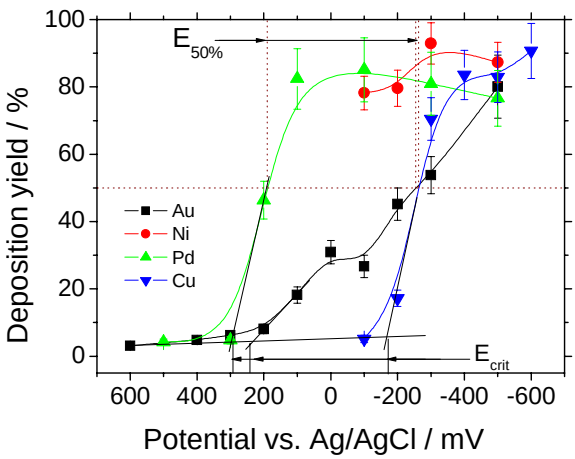

Figure 1: Potential curve for the electrochemical deposition of ^{212}Bi on various electrodes from 0.1 M HCl.

Electrochemical deposition experiments were performed using a potentiostatic setup with an electrochemical cell for fast electrochemical depositions [3]. The electrolyte was 0.1 M HCl, the working electrode material was varied. 1 ml electrolyte containing ^{212}Bi was electrolysed for 10 min, starting at the electrode rest potential which is obtained without applying external current. The deposited activity was measured for 1 min by γ-spectrometry and then electrolysis was resumed at a more negative potential etc.

Table 1: E_{crit} and $E_{50\%}$ values for the deposition of Bi from 0.1 M HCl on various electrode materials

Electrode	E_{crit}	$E_{50\%}$
Au	+250	-240
Pd	+290	+180
Cu	-180	-260
Ni	spontaneous deposition	

Potential curves for the deposition of Bi on Au, Ni, Pd, and Cu are shown in Fig. 1. The critical potential (E_{crit}), at which a significant deposition sets in, and the potential for the deposition of 50 % of the atoms in solution ($E_{50\%}$), are indicated. Numbers are given in Table 1. In agreement with literature [4], a nearly complete deposition of Bi on Ni is already observed at the rest potential (spontaneous deposition). For the deposition on Cu and Pd, s-shaped curves are obtained. The corresponding E_{crit} and $E_{50\%}$ values for the deposition on Pd and Cu differ more than 400 mV, meaning that the interaction of Bi and Pd is much stronger than the interaction of Bi with Cu. The deposition yield for the deposition on Au increases only slowly with decreasing potentials, resulting in a big difference in E_{crit} and $E_{50\%}$. This can be taken as is a sign for a hindrance in the electrodeposition process.

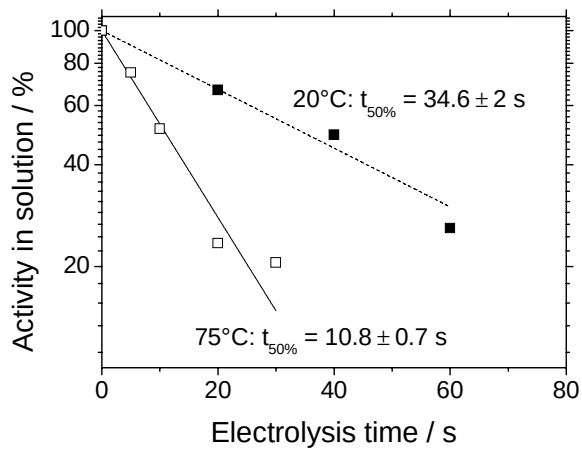

Figure 2: Electrodeposition velocity for the spontaneous electrodeposition of ^{212}Bi on Ni from 0.1 M HCl at room temperature (filled squares) and at 75 °C (open squares).

The electrodeposition velocity was determined for the spontaneous deposition of ^{212}Bi on Ni. Electrolysis was performed for a certain time and the deposited activity was measured. The time for the deposition of 50 % of the atoms in solution ($t_{50\%}$) was 35 s at room temeperature. This value could be lowered to 11 s by increasing the electrolyte temperature to 75 °C.

If isotopes of element 115 with a half-live in the range of 10 s were available, electrodeposition experiments should be performed with Ni or Pd electrodes.

References

[1] H. Hummrich et al., GSI Sci. Rep. 2005, p. 205
[2] H. Hummrich et al., Jahresbericht des Instituts für Kernchemie, Uni Mainz 2002, A10
[3] H. Hummrich et al., GSI Sci. Rep. 2004, p. 188
[4] S.C. Ehinger, R.A. Pacer, F.L. Romines, J. Radioanal. Nucl. Chem. Articles 98, 39 (1986)

First TASCA Commissioning Experiments in the Small Image Size Mode

A. Semchenkov[1,2] , D. Ackermann[1] , W. Brüchle[1] , Ch. E. Düllmann[1] , E. Jäger[1] , E. Schimpf [1] , M. Schädel[1] , J. Dvorak[2] , R.Schuber[2] , A. Türler[2] , A. Yakushev[2] , K. E. Gregorich[3], M. Leino[4] , J. Uusitalo[4], J.-P.Omtvedt[5]

[1]GSI, Darmstadt, Germany; [2] TU Munich, Garching, Germany; [3] LBNL, Berkeley, U.S.A.; [4] JYFL, Jyväskylä, Finland; [5]University of Oslo, Norway

Ion-optical calculations with the code **TRANS**PORT (**TRANS**) (test reaction 235 MeV ^{48}Ca + $^{238}UF_4$ (0.5 mg/cm^2) ==> ^{283}112) were used as a first step to optimize and to built TASCA [1,2]. As a next step the **T**ASCA Monte-Carlo **SIM**ulation program (**TSIM**) was developed and was applied [3] showing good agreement with previous results. Results for TASCA in the **S**mall **Im**age Size **M**ode (**SIM**) are compared in Table 1. Smaller values obtained with the more realistic TSIM are mainly due to straggling and to charge-exchange processes in the gas. A typical product distribution in the focal plane is shown in Figure 1. Based on these simulations we opted for a window with 3 cm in diameter for the SIM **R**ecoil **T**ransfer **C**hamber (**RTC**) [4].

Table 1: Result of TRANSPORT ion-optical calculations and TASCA Monte-Carlo simulations for products from the Ca + U model reaction; see text for details.

Model	TRANS	TSIM
Solid angle / msr	≈ 4.3	≈ 4.2
Transmission / %	≈ 40	≈ 35
Horizontal image size / cm	≈ 3	≈ 4
Vertical image size / cm	≈ 3	≈ 4
Image area / cm^2	≈ 7	≈ 13

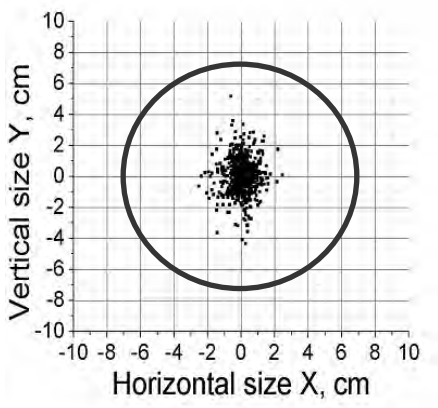

Figure 1: Evaporation residue distribution in the TASCA focal plane obtained from a Monte-Carlo simulation of the ^{48}Ca + ^{238}U model reaction. The circle depicts the 15 cm diameter RTC flange.

First TASCA commissioning experiments in the SIM were successfully performed with the reaction 230 MeV ^{54}Cr + ^{nat}Gd (0.6 mg/cm^2) ==> $^{208-211}$Ra. The Ra distribution in the (8x3.6) cm^2 16-strip silicon **F**ocal **P**lane **D**etector (**FPD**) is shown in Figure 2. Without any significant influence on the transmission the distribution maximum was found 0.5 cm to the left and 0.5 cm below the FPD center position. A comparison between Monte-Carlo simulated and experimental data is shown in Figure 3. The shapes of distributions from the experiment and from TSIM are the same; the smaller number of alphas as compared with recoils is due to a lower efficiency. The 0.5 cm horizontal shift corresponding to ≈ 0.5% in rigidity shows that the dipole magnet settings were slightly off. However, a 0.5% deviation does not influence the experimental result drastically as the momentum acceptance of TASCA in SIM is ± 10% [5]. In general, we observe an excellent agreement between theoretical model calculations and experimental data.

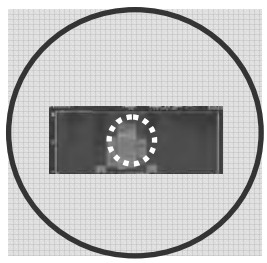

Figure 2: $^{208-211}$Ra distribution (color coded) in the FPD. The reaction was ^{54}Cr + ^{nat}Gd. The circle depicts a 15 cm diameter flange, the dashed line the ø 3 cm RTC window.

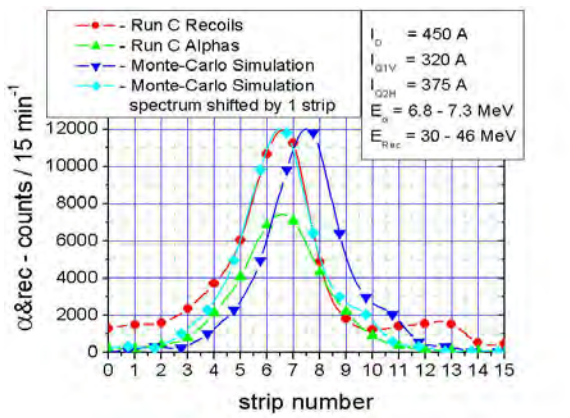

Figure 3: Results from the ^{54}Cr + ^{nat}Gd ==> $^{208-211}$Ra test reaction compared with a Monte-Carlo simulation. Shown is the horizontal distribution in the FPD.

References

[1] A. Semchenkov et al., GSI Scientific Report 2004, p. 332.
[2] M. Schädel et al., GSI Scientific Report 2005, p. 262.
[3] K.E. Gregorich et al., contribution to this report.
[4] Ch.E. Düllmann et al., contribution to this report.
[5] A. Semchenkov et al., contribution to this report.

TASCA as a Preseparator: Recoil Transfer Chamber Commissioning

Ch.E. Düllmann[1,*], D. Ackermann[1], W. Brüchle[1], F.P. Heßberger[1], E. Jäger[1], J. Khuyagbaatar[1], M. Schädel[1], B. Schausten[1], E. Schimpf[1], H.-J. Schött[1], A. Semchenkov[1,2], J. Dvorak[2], A. Gorshkov[2], R. Schuber[2], A. Türler[2], A. Yakushev[2], K. Eberhardt[3], H. Hummrich[3], J.V. Kratz[3], J.P. Omtvedt[4], K. Opel[4], J.M. Gates[5,6], K.E. Gregorich[5], R. Dressler[7], R. Eichler[7,8], Z. Gan[9]

[1]GSI, Darmstadt, Germany; [2]TU Munich, Garching, Germany; [3]U Mainz, Germany; [4]U Oslo, Norway; [5]LBNL, Berkeley, CA, USA; [6]UC Berkeley, CA, USA; [7]PSI, Villigen, Switzerland; [8]U Berne, Switzerland; [9]IMP Lanzhou, P.R. China.

One of the main foreseen applications of the gas-filled TransActinide Separator and Chemistry Apparatus (TASCA) [1] recently installed at GSI is its use as a physical preseparator for chemistry experiments [2,3]; see configuration shown in Figure 1. EVaporation Residues (EVRs) are guided to the focal plane of the separator where they penetrate a thin window separating TASCA's low pressure regime from the 1 bar regime in the Recoil Transfer Chamber (RTC) in which the EVRs are thermalized. Construction of the interface between these two regimes, the RTC window, presents a technical challenge as the following requirements have to be met: i) the window has to withstand the high pressure difference, ii) it has to be gas tight, iii) it has to be so thin that slow EVRs from asymmetric hot fusion reactions can penetrate into the RTC which necessitates using a support grid, and iv) the transparency of this grid has to be high to provide maximum transmission. As has been described before [4] two different ion optical modes are available at TASCA. For both TASCA modes, the Small Image Mode (SIM) as well as the High Transmission Mode (HTM), flanges accommodating RTC windows that match the corresponding image sizes in the focal plane [4] have been built at the TU Munich. Windows made from Mylar foils with thicknesses of 3.3 µm and less are supported by a honeycomb 80%-transparency stainless steel grid. Two RTCs were built, the HTM one (140x40 mm^2) at U Mainz and the SIM one (30 mm ∅) at U Oslo. Both are built in a modular way that allows easy changes of depth and gas flow pattern, see Fig. 2 for the HTM RTC. Additionally, catcher foils can be installed and removed quickly to determine the activity entering the RTC. First commissioning took place in Oct./Nov. 2006 in a ^{40}Ar beamtime.

The HTM RTC was tested with products of the reaction ^{nat}Gd(^{40}Ar,xn)$^{\sim 194}$Pb which were transported with a He/KCl gas-jet to a radiochemical lab located about 13 m away. Aerosol particles were collected on a glass fiber filter that was placed in front of a low energy photon counter for γ counting. Unlike in experiments without preseparation, where the γ spectrum was dominated by lines from unwanted isotopes such as ^{49}Cr or ^{43m,44}Sc produced in reactions of the beam with various parts of the target setup [5], in these tests only γ lines from Pb isotopes and their daughters could be identified, proving the advantage of preseparation. The SIM RTC was tested with short-lived partially α-decaying Hg isotopes from the ^{144}Sm(^{40}Ar,xn)$^{184-x}$Hg reaction. Preseparated Hg atoms were transported with a pure He jet to the Cryo On-line Multidetector for Physics And Chemistry of Transactinides (COMPACT) [6] that registered their α-decay. Only α lines from Hg isotopes and their daughters were visible.

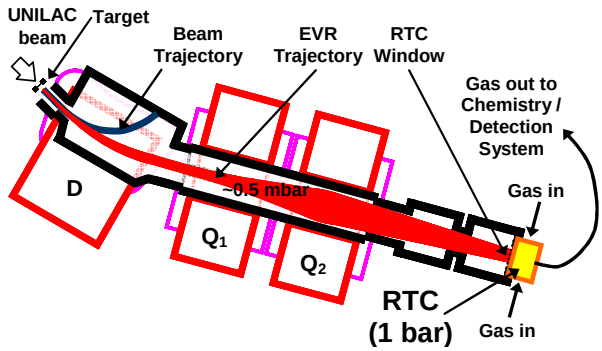

Figure 1: TASCA in the preseparator configuration

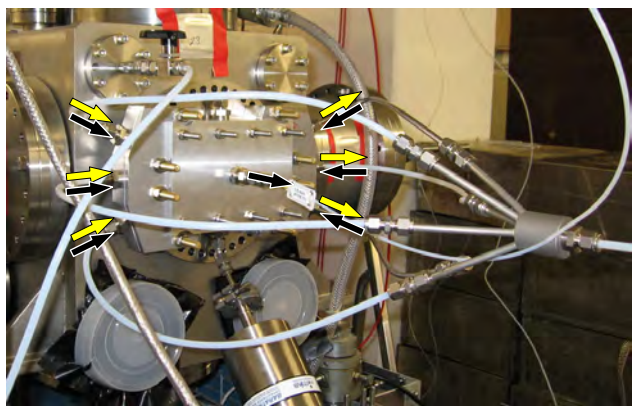

Figure 2: The HTM RTC mounted at TASCA. The two gas flow regimes are indicated by light and dark arrows.

References

[1] M. Schädel *et al.*, GSI Sci. Rep. 2005, Report 2006-1, 2006, p. 262; see also http://www.gsi.de/TASCA.
[2] Ch.E. Düllmann *et al.*, NIM. **A551** (2005) 528.
[3] J.P. Omtvedt *et al.*, J. Nucl. Radiochem. Sci. **3** (2002) 121.
[4] A. Semchenkov *et al.*, GSI Sci. Rep. 2004, Report 2005-1, p. 332.
[5] H. Hummrich, Doctoral thesis, U Mainz, 2006.
[6] J. Dvorak *et al.*, GSI Sci. Rep. 2004, Report 2005-1, p. 183.

Acknowledgements: Thanks to Inge Mikalsen at the University of Oslo and the staff of the mechanical workshop at U Mainz for fast building of the two RTCs.

*c.e.duellmann@gsi.de

Magnetic Field Simulations of the TASCA Magnets

A.Belov[1], T. Belyakova[1], M. Karpakova[1], V. Kukhtin[1], E. Lamzin[1], S. Sytchevsky[1], W. Brüchle[2], E. Jäger[2], E. Schimpf[2], M. Schädel[2], A. Semchenkov[2,3], C. Mühle[2], F. Klos[2], A. Türler[3], A. Yakushev[3]
[1]Efremov Institute, St. Petersburg, Russia, [2]GSI, Darmstadt, Germany; [3] TU Munich, Garching, Germany

To optimize and improve the new separator **TASCA** (**T**rans**A**ctinide **S**eparator and **C**hemistry **A**pparatus) [1], 3D magnetic field measurements and simulations of the TASCA dipole magnet (C-type) and quads were performed.

All field calculations were made with the finite-element code KOMPOT [2, 3]. KOMPOT simulates various 3D stationary field distributions. The code has rich graphic tools (Fig.1, 2) for building finite-element models. The postprocessor is capable to produce distributed and integral magnetic characteristics. For example, field maps or magnetic fluxes and EM forces for a given region are created. The graphical interface makes it possible to visualize calculated field distributions in any region of interest and to compare it with data measured at the GSI.

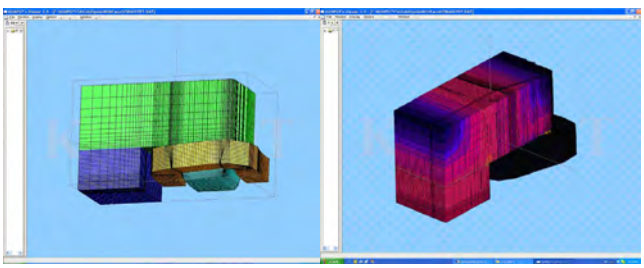

a) b)

Figure 1:a) 3D-graphic presentation of the C-magnet; b) Magnetic field distribution on the magnet surface.

The model developed for the C-magnet was reduced to one quarter of the magnet (Fig.1). The mesh had ≈0.5M nodes. More than 30 runs were carried out: a) with currents varying from 50 A to 700 A; b) with 700 A to optimize pole shapes; c) for the optimized poles shape with the currents up to 850 A.

Comparisons between measurements and simulations show good agreement. Computational model and magnetic measurement data allow calculating magnets with required magnetic field distributions. In addition, the synergism between model calculation and measurement does yield much better and much more economic results in magnet design and optimization. The magnetic field simulations provide the 3D field map in the working area of the dipole magnet and the corresponding optical characteristics for the entire envisioned induction (current) range.

In addition 3D field simulation has been performed for the quadrupoles [2, 3] in order to obtain magnetic field maps for (i) a single quadrupole magnet, (ii) two quads turned by 90 degrees relative to each other around their common axis and (iii) two quads taking into account the magnetic permeability of the duct and a valve (Fig.2).

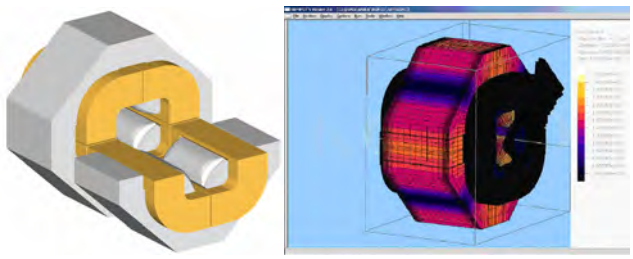

a) b)

Figure 2: a) Computational model of a doublet of quads. b) Magnetic field distributions on the surfaces of a single quadrupole with a valve.

The calculation mesh of doublet of quads contains ≈0.5M finite elements (Fig.2a). This model was used as reference to calculate the field for a set of coil currents from 200 to 650 A. The FE model allowed calculation of a precise field map for two nearby quads. The 3D field distribution was obtained in each quad, in between quads and in the region from the quad edge to the external boundary. The field of a single quad can be assessed assuming negligible interference of the magnet ends.

The second calculation model accounts for the influence of the duct and the vacuum valve (Fig.2b). Direct subtraction of field maps obtained with two different models (with and without the duct) using the same FE mesh revealed minor deviations of field and field gradient in the working area of the quads. Both the field and gradient deviations were found to be below 0.05%. As the vacuum valve introduces an asymmetry in the magnet system, an FE mesh should be built over the entire R^3 area that necessitates significant increase in computational resources. To study the influence of the valve a dedicated FE model was developed. The model has $>0.4\cdot10^6$ finite elements. From the measured data provided by GSI, the vacuum valve permeability was taken constant as μ_{VL}=1.4. An additional calculation at μ_{VL}= 1.0 gave assessment for the vacuum valve influence. The resultant field deviations with valve and without valve in the working area were as low as ΔB = 2 G, and deviations of the field gradient were within 0.1%.

The calculated field maps were used as inputs for the TASCA trajectory analysis.

References

[1] M. Schädel et al., GSI Scientific Report 2005, p. 262.
[2] A.Belov, et al., KOMPOT/M 1.0: computer code for 3D simulation of magnetostatic field, RF Registration Certificate N2003612492
[3] N.I.Doinikov, et al., On computation of 3-D magnetostatic fields of electrophysical apparatus magnet systems, IEEE Transact. On Magnetics, v.28, No.1, January 1992, pp.908–911C.

TASCA Monte-Carlo Simulation Program and Program for Studying Ion-Optical Parameters of Dipole and Quadrupole Magnets from Field Maps

K.E. Gregorich[1], A. Semchenkov[2,3], T. Belyakova[4], V. Kukhtin[4], E. Lamzin[4], S. Sytchevsky[4], W. Brüchle[2], Ch. E. Düllmann[2], E. Jäger[2], E. Schimpf[2], M. Schädel[2], J. Dvorak[3], A.Türler[3], A. Yakushev[3]

[1]LBNL, Berkeley, U.S.A., [2]GSI, Darmstadt, Germany; [3]TUM, Garching, Germany; [4]Efremov Institute, St. Petersburg, Russia

Ion-optical calculations are often performed as a first step when designing magnetic systems. As a second step Monte-Carlo simulations are performed of **EV**aporation **R**esidue (**EVR**) trajectories through the separator, varying parameters like target thickness, gas pressure and magnet field. Such a program is very useful to optimize all system parameters and to plan and to prepare experiments.

The new **T**ASCA Monte-Carlo **SIM**ulation program (**TSIM**) is based on the **B**erkeley Gas-filled Separator **SIM**ulation program (**BSIM**) [1]. TSIM uses magnetic field maps of the TASCA dipole and quadrupole magnets, simulated by the program KOMPOT [2].

Trajectories are simulated in three steps. As a first step the event generator code **TRIMIN** (**TRIM IN**put code) generates EVRs in the target material. The following tools and input parameters are used to characterize these EVRs: a) the energy loss for the primary beam in the target material is calculated by SRIM [3] or LISE [4]; b) Gaussian type distributions with realistic widths are assumed for the primary beam energy and angular spread; c) a beam energy is randomly chosen within the excitation function for every EVR birth. A depth in the target material corresponding to this energy is determined; d) initial position of compound nuclei trajectories and recoil energies are simulated. They are modified by neutron evaporation with a kinetic energy of ~2 MeV emitted in random direction.

As an output TRIMIN gives recoil energies, position distributions and angular distributions for the EVRs inside the target, which are used as an input for the second step of the simulation process. Here EVRs are transmitted from their initial target position through remaining target material using the SRIM code [3]. The output file with recoil energy distributions and angle distributions of EVRs exiting the target serves as an input file for the last step of the TSIM calculation. This part of the simulation program, based on the original BSIM program, was adapted for TASCA taking especially into account the TASCA geometry like target position, dimensions of ducts and the detector position with variations of the detector size. Transmitting EVRs through the gas-filled separator, straggling, energy loss and charge-exchange are taken into account.

Fig.1 shows simulated trajectories of EVRs from the Ca + U reaction with TASCA; i.e. the dipole magnet followed by the first horizontally focusing quad and the second vertically focusing one; see refs. [5, 6] for more information. TSIM can be used to optimize target thickness or duct shapes and it can also be used to find the best gas pressure for a specific reaction and magnet settings.

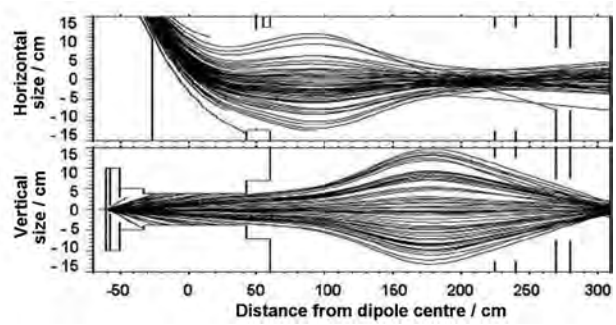

Figure 1: EVR trajectory simulations in TASCA projected in the horizontal (upper panel) and vertical (lower panel)

The newly developed KOMPOT [2] postprocessors allow calculating ion-optical parameters of the dipole magnet (**MOPS** code – **M**agneto-**O**ptical **P**arameters **S**imulation) and of quads (MOPS2 code) from field maps of the working area of the magnets. As program input data we have used the magnetic field map. The dipole magnet parameters calculated by MOPS are: a) magnetic field distribution and its series expansion in the medium plane; b) magnetic length distribution and its series of expansion in dependence on radius c) bending angle for the central trajectory and bending angle distributions at the entry and the exit; d) series of expansion for bending angles; g) edge angle distribution and the series of expansion at the entry and at the exit of the magnet; e) field distribution along the central trajectory; f) series of expansion for edge field at the entry and at the exit of the magnet.

MOPS2 allows determining ion-optical parameters of quads, based on calculated or measured distribution of magnetic field in the working area of the quads, such as: a) magnetic field and field gradient in the middle point; b) magnetic field and gradient distribution in the medium plane; c) series of expansion for field and gradient distributions; d) magnetic length for the central trajectory; e) magnetic length distribution depends on extension from the central axis; f) series of expansion for magnetic length; h) field gradient distribution on the central trajectory.

References

[1] K.E. Gregorich et al. Eur. Phys. J. A 18, 633 (2003).
[2] A. Belov et al., contributions to this report.
[3] J.F. Ziegler, Nucl. Instr. and Meth. in Phys. Res. B 219, 1027 (2004).
[4] O.Tarasov, D.Basin, LISE++ home page. ftp://ftp.nscl.msu.edu/pub/lise
[5] A. Semchenkov et al., contributions to this report.
[6] Ch.E. Düllmann et al., contributions to this report.

Radioactive Targets for TASCA

K. Eberhardt[1], J. V. Kratz[1], D. Liebe[1], P. Thörle[1], W. Brüchle[2], Ch. E. Düllmann[2], W. Hartmann[2], A. Hübner[2], E. Jäger[2], B. Kindler[2], B. Lommel[2], R. Mann[2] , M. Schädel[2], B. Schausten[2], E. Schimpf[2], A. Semchenkov[2,6], J. Steiner[2], K. E. Gregorich[3], H.-J. Maier[4], J. Szerypo[4], R. Sudowe[5], A. Türler[6], A. Yakushev[6]

[1]Johannes Gutenberg-Universität Mainz, Germany (UMZ); [2]GSI, Darmstadt, Germany; [3]Lawrence Berkeley National Laboratory, Berkeley, USA (LBNL); [4]Ludwigs-Maximilians-Universität München, Germany (LMU); [5]University of Nevada, Las Vegas, USA (UNLV); [6]Technische Universität München, Germany (TUM)

The main components of the **T**rans**A**ctinide **S**eparator and **C**hemistry **A**pparatus **TASCA** are already installed and the separator is now in the commissioning phase. A first beam time took place in April 2006 and further commissioning experiments were performed in May and November 2006. An overview of the current status is given in separate contributions [1,2].

For the beam time in May a number of different target materials have been applied, among them a set of ^{nat}Gd-targets produced by Molecular Plating at UMZ on a 5 µm Ti-backing foil. The targets withstood a 1.43 μA_{part} Cr^{7+}-beam without damage although the use of a relatively thick Ti-backing resulted in an increased background signal. One main goal of the experiment in November was the test of different ^{238}U-targets with an intense $^{40}Ar^{10+}$-beam. Two target wheels have been irradiated – TN4 and TN8 – both consisting of three different kinds of targets.

All targets have been delivered by the GSI target laboratory. Here, the U-layer of about 500 µg/cm^2 has been produced by sputtering of depleted uranium in its metallic form with an ^{235}U content less than 0.2% [3]. Here, C and Ti, respectively, have been used as a backing material. In some cases the U-layer has been covered with a thin C layer in order to prevent losses of the target material during irradiation with the $^{40}Ar^{10+}$-beam. After a certain beam integral was applied, the targets have been inspected to check for damage. Target wheel TN4 has first been irradiated for a total of about one hour with increasing beam intensity up to 2 μA_{part}. The target segments showed severe damage with holes and cracks. TN4 was then replaced by TN8 which was irradiated for about 1.5 hours with increasing beam intensities up to 1 μA_{part}. Figure 1 shows TN8 before and after irradiation, respectively. After irradiation segment 1 (C-backing/C cover) showed a visible hole, whereas segments 2 and 3 (Ti-backing) remained mechanically stable but show intense colour changes in the central part (see fig.1).

In order to check for material losses and homogeneity, the targets with Ti-backing are currently inspected by radiographic imaging using a FLA 7000 Imager from FUJIFILM Corporation. Figure 2 shows a radiographic image of target segment #3 from target wheel TN8 with a U-content of 491µg/cm^2. Here, light grey areas correspond to the initial deposited and uniformly distributed U-layer. The dark grey area in the center part indicates the $^{40}Ar^{10+}$-beam track. Here, the higher activity origins from an activation of the Ti-backing and the U target material by the beam. Information about material losses due to the interaction with the beam is not yet available. Thus, work is currently in progress at GSI to produce U-samples as a calibration standard for quantitative measurements of target thicknesses using radiographic imaging. The targets are further inspected by α-particle counting of the U-layer in order to check for material losses. Furthermore, the targets will be inspected by electron beam diagnostics.

Figure 1: Target TN8 before (left) and after irradiation (right) with a $^{40}Ar^{10+}$-beam of 1 μA_{part} maximum intensity.

Figure 2: Radiographic image of target segment # 3 from target wheel TN 8. See text for details.

At UMZ work is currently under way to find optimum conditions for the deposition of ^{244}Pu (up to 500 µg/cm^2) on 2 µm thin Ti backing foils by Molecular Plating from isobutanolic solution. ^{244}Pu is of special interest as a target material for chemical investigations of the heaviest elements, since relatively long lived isotopes of Rf to Hs - with half-lives in the order of a few seconds - can be produced in the bombardment of a ^{244}Pu-target with beams ranging from ^{22}Ne up to ^{30}Si. ^{244}Pu is also the optimum target for production of Z=114 with a ^{48}Ca beam.

References

[1] A. Semchenkov et al., contribution to this report
[2] Ch. E. Düllmann et al., contribution to this report
[3] B. Kindler et al., contribution to this report

See also http://www.gsi.de/TASCA

Fully Relativistic *ab initio* Dirac-Coulomb Calculations of Atomic Properties of Hg and Element 112

V. Pershina[1], A. Borschevsky[2], E. Eliav[2], and U. Kaldor[2]
[1]GSI, Darmstadt, Germany; [2]Tel Aviv University, Israel

For accurate calculations of the electronic structures of the heaviest elements and their compounds, where relativistic effects are of paramount importance, the usage of fully relativistic quantum chemical methods within 4-component approximation is highly desirable. Such a usage encountered until recently difficulties for many electron systems with respect to the treatment of the electron correlation. Meanwhile, this problem has been tackled, and the latest version of the DIRAC package offers possibility of calculating the electronic structure of the heavy element compounds using the DC (Dirac-Coulomb) Hamiltonian and treating the electron correlation at various levels of theory including the most sophisticated, such as the Coupled Cluster Single Double (Triple) excitations [CCSD(T)] [1]. Meanwhile, optimal basis sets for the heaviest elements have also been developed [2]. In this work, we have made use of the recent developments in the DIRAC program and calculated atomic properties of Hg and element 112 at a very advanced level of theory.

In the basis of the DC method lies the many-electron relativistic Dirac-Coulomb Hamiltonian

$$H_{DC} = \sum_i h_D + \sum_{i<j} 1/r_{ij} \,, \qquad (1)$$

where

$$h_D = c\vec{\alpha}\cdot\vec{p} + \beta c^2 + V_{nuc} \,. \qquad (2)$$

The atomic orbitals are four-component spinors

$$\phi_{nk} = \begin{pmatrix} P_{nk}(r) \\ Q_{nk}(r) \end{pmatrix} , \qquad (3)$$

where $P_{nk}(r)$ and $Q_{nk}(r)$ are large and small component, respectively. The Faegri uncontracted 26s23p18d13f5g2h basis set was used for element 112 [2], while the Visscher polarized basis sets was used for Hg [3].

The calculations of polarizability (α) were performed at the DC single reference CCSD(T) level with the use of the finite field method. The strengths of the field were chosen as 0.0001, 0.001 and 0.01 a.u. Results for α are given in Table 1 along with the other best calculated properties of Hg and element 112. These properties are needed for calculations of the energy of physisorption of these elements on inert surfaces like quartz or ice. Ionization potentials (IP) were calculated at the Dirac-Coulomb-Breit Fock-Space CC (DCB FSCC) level [4]. The atomic radii (AR) were determined as a half of the bond lengths R_e in the dimers Hg_2 and $(112)_2$ calculated using the 4c-DFT method (4-component Density Functional Theory method, the spin-polarized version, non-collinear approximation) [5,6]. Also, AR calculated on the basis of R_{max} of the outer electron orbital are similar [7]. Results are summarized in Table 2. For comparison, non-relativistic values are also given there.

Table 1. Atomic properties of Hg and element 112 needed for calculations of the energy of physisorption

Property	Hg		Ref.	element 112		Ref.
	nr	rel		nr	rel	
IP, eV	8.98	10.44	cal.[4]	8.25	11.97	cal.[4]
		10.43	exp.			
α, a.u.	57.83	33.94	this		25.38	this
		33.91	exp.[8]	74.66	25.8	cal.[9]
AR, a.u.	3.91	3.43	calc. [6]	4.32	3.26	[6]
		3.43	exp.[10]		3.22	[7]

One can see that agreement between the present calculated DC CCSD(T) and experimental value [8] for α(Hg) is excellent. This guarantees high accuracy of the results for element 112. With the newly calculated values of IP, α and AR, the energy of physisorption of Hg and element 112 on quartz was calculated as ΔH_{ads}(Hg) = -40.8 kJ/mol using a model of atom-slab interaction [7]. This value agrees very well with the measured ΔH_{ads}(Hg) = -42 ± 2 kJ/mol. Accordingly, ΔH_{ads}(112) = -45.8 kJ/mol. The obtained results indicate that relativistically, element 112 will be stronger adsorbed on inert surfaces than Hg. Non-relativistically, ΔH_{ads}(112) = -40.2 kJ/mol, which means that non-relativistically, element 112 would have been less strongly adsorbed than Hg. Thus, relativistic effects make element 112 less, not more, volatile than Hg upon adsorption on inert surfaces.

References

[1] DIRAC 04, written by H.J. Ja. Jensen, *et al*. (2004).
[2] K. Faegri, Theor. Chim. Acta, 105 (2001) 252 .
[3] L. Visscher, private communication.
[4] U. Kaldor and E. Eliav, Adv. Quant. Chem. 31 (1998) 313.
[5] J. Anton *et al*. Phys. Rev. A 69 (2004) 012505.
[6] J. Anton *et al.* Chem. Phys. 311 (2005) 97.
[7] V. Pershina and T. Bastug, Chem. Phys. 311 (2005) 139.
[8] D. Goebel and U. Hohm, J. Phys. Chem. 100 (1996) 7710.
[9] M. Seth, Doctoral Thesis, University of Auckland, 1998.
[10] R. D. See, *et al.* J. Chem. Phys. 88 (1988) 4650.

Non-collinear relativistic DFT calculations for small molecules with superheavy elements 111 and 113

C. Sarpe-Tudoran[1], J. Anton[1], B. Fricke[1], V. Pershina[2]
[1]Universität Kassel, Institut für Physik, 34109 Kassel, Germany; [2]GSI Darmstadt, Germany

During the last 15 years a lot of effort has been invested in the experimental investigation of the chemical behaviour of superheavy elements. One was able to show that the general feature of the elements 104 to 108 is to follow the trend of the continuation of the Periodic Table [1]. Details of the experimental methods and results can be found in the recent review by Schädel [2].

These elements are so heavy that any non-relativistic calculation can not give a realistic prediction so that a full relativistic calculation is the only appropriate method. Details of the theoretical methods and results can be found in the review by Pershina [3].

The theoretical as well as the experimental effort now concentrates on the investigation of the chemical behaviour of the elements beyond 110. In this region of elements up to now nothing is known experimentally. The nuclear chemists concentrate on the chemistry of element 112. They have set up an experiment to investigate the adsorption of this element relativ to the homologue Hg and the noble gas Rn. Positive results of those experiments have recenly been reported [4].

During the last years we have investigated theoretically the adsorption energy of element 112 and Hg on a Au surface. The newest results predict an adsorption energy of about 0.7 eV [5] which is somewhat below Hg but reasonably higher than that of Rn.

Because all these elements between 110 and 119 now become interesting, the effort from the theoretical side concentrates on the calculation of small molecules with superheavy elements. These kind of calculations together with analogue calculations for their homologues allow further predictions of their chemical behaviour. Various methods have been used so far. A few references including results for even heavier elements can be found in Ref. [6-10].

Our method of calculation is a full relativistic 4-component molecular code which now includes the possibility to calculate these systems in a non-collinear fashion. This method allows the magnetic density distribution to show in different directions in different regions of the molecule. This is connected with different total energies and thus modifies the binding energies of the molecules compared to the collinear method which is used up to now.

Table 1 lists the binding energies D_e, the bond distances R_e and frequencies ω_e for a few superheavy molecules with element 111 and 113. For the diatomic molecule $(111)_2$ the potential energy curve in different approximations is given in Fig. 1. These values are important ingredients in order to understand the chemical behaviour of these elements which are dominated by large direct relativistic effects for the $7p_{1/2}$ electrons and large spin-orbit splitting of the 7p-shell in the case of element 113.

Table 1: Bond lengths, R_e, bond energies, D_e, and vibration frequences, ω_e, for a number of diatomic molecules of elements 111 and 113

Molecule	R_e (Å)	D_e (eV)	ω_e (cm^{-1})
(111)H	1.52	2.85	2804
(111)F	1.94	2.65	597
(111)Au	2.57	1.34	150
(113)H	1.78	1.70	1606
(113)F	2.23	3.42	375

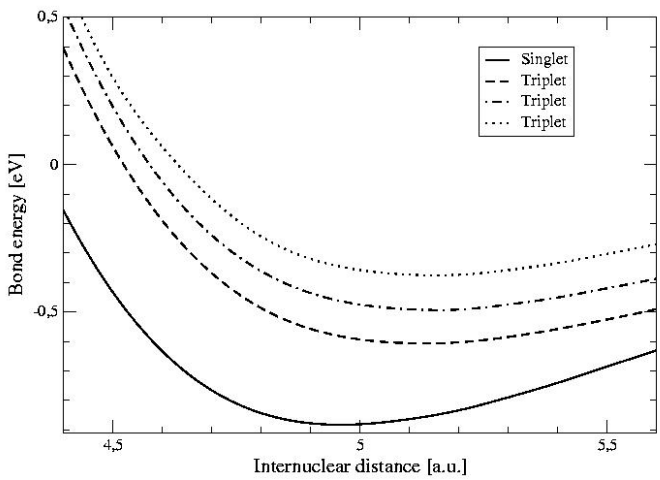

Figure 1: Potential energy curve for the system $(111)_2$ with a large triplet splitting

References

[1] B. Fricke, Struct. Bond. 21 (1975) 89.
[2] M. Schädel, Angew. Chem. Int. Ed. 45 (2006) 368.
[3] V. Pershina, Chem. Rev. 96 (1996) 1977.
[4] H. W. Gäggeler, R. Eichler PSI Press release 31. May 2006.
I5] C. Sarpe-Tudoran *et al.*, J. Chem. Phys., submitted.
[6] M. Seth et al., Chem. Phys. Lett. 250 (1996) 461; J. Chem. Phys. 106 (1997) 3623; 109 (1998) 3935; 111 (1999) 6422.
[7] J. Anton *et al.*, Chem. Phys. 311 (2005) 97.
[8] W. Liu *et al.*, J. Chem. Phys. 116 (2002) 3626.
[9] N. S. Mosyagin *et al.*, J. Chem. Phys. 124 (2006) 224302.
[10] C. S. Nash *et al.*, J. Phys. Chem. A 103 (1999) 632.

Fully Relativistic Density-Functional-Theory Calculations for Intermetallic Compounds of Pb and Element 114

V. Pershina[1], J. Anton[2], B. Fricke[2]
[1]GSI, Darmstadt, Germany; [2]University of Kassel, Germany

Theoretical predictions of adsorption behaviour is very important for chemical identification of the heaviest elements using gas-phase chromatography techniques or electrochemical deposition from aqueous solutions. Earlier, we have predicted the adsorption enthalpy ΔH_{ads} and the temperature T_{ads} for element 112 with respect to that of Hg on gold (100) surface [1,2]. Recent experiments have confirmed theoretically predicted similarity of element 112 with Hg [3]. This work is an initial step in the long-term project on predicting adsorption behaviour of element 114 with respect to that of Pb on various metal surfaces. Here, we present calculations of binding energies D_e and other spectroscopic properties of the dimers of Pb and element 114 with group 10, 11 and 14 elements.

The calculations were performed using the 4-component Density Functional Theory method (4c-DFT) in the spin-polarized version (non-collinear approximation) [4]. The results for group 10 and 11 dimers are summarized in Table 1. Results for the dimers of Pb and element 114 with group 14 elements are given in Table 2.

Table 1. Optimized bond lengths (R_e), binding energies (D_e) and harmonic vibrational frequencies (w_e) for PbM and 114M, where M are group 10 and 11 elements

Molecule	R_e, a.u.	D_e, eV	w_e, cm^{-1}
PbNi	4.50	1.80	-
PbPd	4.73	1.95	201.77
PbPt	4.63	3.53	213.49
PbCu	4.80	1.60	-
PbAg	5.05	1.22	-
PbAu	4.99	2.15	152.73
114Ni	4.70	0.25	-
114Pd	5.08	0.79	137.82
114Pt	4.84	1.11	157.37
114Cu	5.20	0.47	-
114Ag	5.50	0.30	-
114Au	5.44	0.73	96.70

The results of Table 1 show that element 114 should form relatively strong bonding with the group 10 and 11 transition elements which is about 1 eV weaker than that of the corresponding Pb compounds. Bonding of both Pb and element 114 with Pt should be the strongest among these transition metals, while that with Ag should be the weakest. With group 14 elements (Table 2), Sn and Pb, element 114 should also form rather strong bonding, about 1 eV weaker than that of Pb. R_e of the 114 compounds are respectively longer. The bond in $(114)_2$ is stronger than the pure van der Waals one (Fig. 1).

Table 2. Optimized bond lengths (R_e), binding energies (D_e) and harmonic vibrational frequencies (w_e) for PbM and 114M, where M are group 14 elements

Molecule	R_e, a.u.	D_e, eV	w_e, cm^{-1}	Ref.
PbSn	5.50	2.93	-	this
PbPb	5.62	1.18	107	this
	5.53	0.86±0.01	110	exp. [5]
114Sn	5.80	1.83	-	this
114Pb	6.00	0.406	-	this
(114)(114)	6.60	0.13	26	this

The present results show similar trends for D_e, R_e, and w_e of PbM and 114M as a function of the second metal atom M. The trends in D_e for PbM are also similar to ΔH_{ads} of Pb on the corresponding metal surfaces [6]. The calculated D_e for the dimers can be used for first estimates of $\Delta H_{ads}(114)$ on the corresponding metal surfaces, as it was done for element 112 [7]. We share the opinion of [8] that the DFT results for various systems are systematic and offer consistent trends in properties.

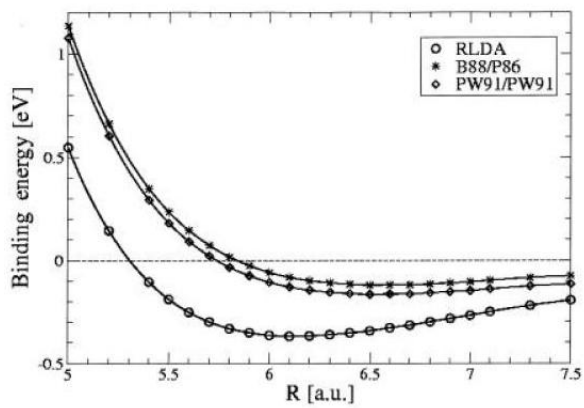

Fig. 1. Binding energy of $(114)_2$ as a function of the bond length R_e calculated in various DFT approximations. The highest level of approximation is B88/P86.

References

[1] V. Pershina *et al*. Nucl. Phys. A734 (2004) 200.
[2] C. Sarpe-Tudoran, J. Chem. Phys. submitted.
[3] H.W. Gäggeler, R. Eichler *et al*., PSI press release 31. May 2006.
[4] J. Anton *et al*. Phys. Rev. A 69 (2004) 012505.
[5] K. Pitzer *et al*. J. Phys. Chem. 86 (1982) 3068.
[6] F. Haenssler *et al*. PSI Annual report 2005, p. 3.
[7] V. Pershina *et al*. Chem. Phys. Lett. 265 (2002) 176.
[8] W. Liu *et al*. Adv. Quant. Chem. 39 (2001) 325.